PERGAMON

Building and Environment 36 (2001) 871–882

BUILDING AND ENVIRONMENT

www.elsevier.com/locate/buildenv

Thermal stratification produced by plumes and jets in enclosed spaces

G.R. Hunt[a,*], P. Cooper[b], P.F. Linden[c]

[a] *Department of Civil and Environmental Engineering, Imperial College of Science, Technology and Medicine, London, SW7 2BU, UK*
[b] *Faculty of Engineering, University of Wollongong, New South Wales, 2522, Australia*
[c] *Department of Mechanical and Aerospace Engineering, University of California, San Diego, 9500 Gilman Drive, La Jolla, CA 92093-0411, USA*

Abstract

The airflow and thermal stratification produced by a localised heat source located at floor level in a closed room is of considerable practical interest and is commonly referred to as a 'filling box'. In rooms with low aspect ratios $H/R \lesssim 1$ (room height H to characteristic horizontal dimension R) the thermal plume spreads laterally on reaching the ceiling and a descending horizontal 'front' forms separating a stably stratified, warm upper region from cooler air below. The stratification is well predicted for $H/R \lesssim 1$ by the original filling box model of Baines and Turner (J. Fluid. Mech. 37 (1968) 51). This model represents a somewhat idealised situation of a plume rising from a point source of buoyancy alone—in particular the momentum flux at the source is zero. In practical situations, real sources of heating and cooling in a ventilation system often include initial fluxes of both buoyancy and momentum, e.g. where a heating system vents warm air into a space. This paper describes laboratory experiments to determine the dependence of the 'front' formation and stratification on the source momentum and buoyancy fluxes of a single source, and on the location and relative strengths of two sources from which momentum and buoyancy fluxes were supplied separately.

For a single source with a non-zero input of momentum, the rate of descent of the front is more rapid than for the case of zero source momentum flux and increases with increasing momentum input. Increasing the source momentum flux effectively increases the height of the enclosure, and leads to enhanced overturning motions and finally to complete mixing for highly momentum-driven flows. Stratified flows may be maintained by reducing the aspect ratio of the enclosure. At these low aspect ratios different long-time behaviour is observed depending on the nature of the heat input. A constant heat flux always produces a stratified interior at large times. On the other hand, a constant temperature supply ultimately produces a well-mixed space at the supply temperature.

For separate sources of momentum and buoyancy, the developing stratification is shown to be strongly dependent on the separation of the sources and their relative strengths. Even at small separation distances the stratification initially exhibits horizontal inhomogeneity with localised regions of warm fluid (from the buoyancy source) and cool fluid. This inhomogeneity is less pronounced as the strength of one source is increased relative to the other. Regardless of the strengths of the sources, a constant buoyancy flux source dominates after sufficiently large times, although the strength of the momentum source determines whether the enclosure is initially well mixed (strong momentum source) or stably stratified (weak momentum source).

Keywords: Thermal stratification; Closed room; Localised heat source; Source momentum flux; Aspect ratio

1. Introduction

The thermal stratification generated by a localised source of heat at floor level in a confined space is of considerable interest to building ventilation. Many sources of heat generation in buildings may be regarded as being localised, e.g. computers, occupants etc., and knowledge of the developing vertical temperature profile produced by these sources is required before air quality and occupant comfort levels can be determined. In general, these sources may be classified as either '*pure*' buoyancy sources, e.g. an electric fire or a radiator in a hot water heating system, or as '*forced*' buoyancy sources which are characterised by non-zero source momentum fluxes, e.g. in a heating system in which warm air is injected into the space.

The stratification produced by a localised *pure* heat source in an unventilated enclosure that initially contains cool air of a uniform temperature has been considered by Baines and Turner [1]; referred to hereafter as B&T. Using a saline

* Corresponding author.
E-mail address: gary.hunt@ic.ac.uk (G.R. Hunt).

0360-1323/01/$ - see front matter
PII: S0360-1323(01)00013-0

Nomenclature

A_S	Area of source (m^2)
Ar	Archimedes number
$Ar(0)$	Source value of the Archimedes number
b	Plume radius (m)
B_0	Buoyancy flux of the source ($m^4\ s^{-3}$)
B	Total buoyancy of upper layer formed initially ($m^4\ s^{-2}$)
c_p	Specific heat capacity ($j\ kg^{-1}\ C^{-1}$)
c, c_2	Dimensionless plume parameters dependent on the entrainment coefficient
d_{max}	Maximum penetration depth of the buoyant intrusion (m)
E	Heating load of the source (W)
g	Acceleration due to gravity ($m\ s^{-2}$)
g'	Reduced gravity of the source ($m\ s^{-2}$)
g'_i	Reduced gravity of the interior ($m\ s^{-2}$)
G	Constant, ≈ 1.159
H	Enclosure height (m)
H_{eff}	Effective height of enclosure (m)
I	Inertia of plume at the ceiling ($m^4\ s^{-2}$)
$2L_1, 2L_2$	Horizontal dimensions of enclosure (m)
L_j	Jet-length (m)
L_q	Length scale characterising importance of source flow rate in a plume
M	Momentum flux ($m^4\ s^{-2}$)
M_0	Momentum flux of the source ($m^4\ s^{-2}$)
Q	Volume flow rate ($m^3\ s^{-1}$)
Q_0	Volume flow rate of the source ($m^3\ s^{-1}$)
R	Characteristic horizontal enclosure dimension (m)
S	Cross-sectional area of enclosure (m^2)
t	Time (s)
t_n	time constant, $= V/Q_0$ (s)
t^*	Characteristic time scale, $= gV/B_0$ (s)
T_i, T_0	Internal temperature (°C) at time t, initial temperature (K) (= initial temp. °C + 273)
U_w	Velocity in ceiling current at point of impact with side wall ($m\ s^{-1}$)
V	Volume of enclosure (m^3)
z	Vertical co-ordinate (m)
z_0	Height of first front above actual source (m)
z_v	Vertical distance between actual and virtual sources (m)
α	Entrainment coefficient
β	Coefficient of thermal expansion ($°C^{-1}$)
$\Delta\rho$	Density contrast between plume fluid at source and surroundings ($kg\ m^{-3}$)
χ	Horizontal source separation (m)
ϕ	Source diameter (m)
ρ	Fluid density ($kg\ m^{-3}$)
σ	Empirical constant, $= 1.85$
τ	Characteristic time scale (s)

Subscripts

c	refers to quantities in the ceiling current
i	refers to quantities in the interior
s	refers to quantities at the supply
0	refers to initial quantities

plume in a water tank as a model for a heat source in air,[1] B&T observed and measured the developing vertical stratification. Their experiments showed that for a range of aspect ratios H/R (room height H to characteristic horizontal dimension R) the rising turbulent plume spreads across the ceiling to form a warm layer of air, separated by a horizontal initial 'front' (or thermal interface) from the layer of cooler air below. Turbulence in the warm upper layer decays and the spreading warm air becomes part of the non-turbulent environment. Subsequently, the plume rises through this growing warm layer and arrives at the ceiling warmer than it did before. As a result, the outflow from the plume is warmer and occurs *above* the existing warm region that is displaced downwards and a stable stratification develops. B&T tracked the position of the initial front and, using plume theory (Morton et al. [2]), showed that the relationship between front height $z = z_0$ above floor level and the time t after the plume first reached the ceiling is closely predicted by the expression

$$\frac{z_0}{H} = \left[\frac{4\alpha}{5}\left(\frac{18\alpha}{5\pi}\right)^{1/3}\frac{tH^{2/3}B_0^{1/3}}{R^2} + 1\right]^{-3/2} \quad \text{for } H/R < 1, \tag{1}$$

where B_0 denotes the buoyancy flux of the source and α (≈ 0.083, Turner [3]) is an empirically determined plume entrainment coefficient. At large aspect ratios H/R, B&T observed that the initial outflow from the plume intruded vertically downwards into the cooler layer below after colliding with the side walls of the container, and that this intrusion was re-entrained by the plume. This resulted in mixing and a general overturning motion that increased in scale as H/R increased. The (stabilising) buoyant ceiling layer opposes the (destabilising) momentum flux generated by the plume, and B&T argued that if this momentum flux could be deflected downwards, a measure of the tendency towards overturning is the ratio of the inertia and buoyancy forces $I/\mathbf{B}$, namely,

$$\frac{I}{\mathbf{B}} = \frac{9\alpha}{10}\left(\frac{H}{R}\right)^2. \tag{2}$$

[1] Throughout this paper the results of laboratory experiments are described as though for heat rising in air. Images of the flows observed during experiments are shown as seen in the laboratory.

B&T found $H/R \approx 1$ to be the maximum value for which the filling box model (1) holds and, thus, the limiting value of the parameter $I/\mathbf{B}$ in (2) is approximately 0.1, i.e. the inertia force need only be about 10% of the buoyancy force to prevent the filling box behaviour. For $H/R < 1$, the depth of the layer formed by the initial plume outflow is small compared with H and overturning motions are negligible. For larger aspect ratios ($1 \lesssim H/R \lesssim 6$) an increasing pattern of overturning is observed with increasing H/R, and the geometry of the space plays a significant role in encouraging mixing. For $H/R \gtrsim 6$, the stratification changes dramatically from that of the filling box (Barnett [4]).

B&T consider the stratification established by a *pure* source of buoyancy. In practical situations, however, real sources of heating and cooling in a ventilation system often include initial fluxes of both buoyancy and momentum. With combined buoyancy and momentum inputs, a number of questions arise, such as how does the balance between the buoyancy and momentum of a single source or supplied individually from two separate sources affect the mixing, stratification and air quality in a room? To determine the dependence of both the 'front' formation and stratification on the source momentum M_0 and buoyancy B_0 fluxes new experiments were performed. First, the case of an enclosure containing a *forced* buoyancy source was considered. We then further extended the concept of a filling box with an input of momentum by considering an enclosure containing two localised sources, namely, a source of momentum flux only (a jet) and a source of buoyancy flux only (a plume). The primary motive for considering this latter configuration of sources was to determine how the stratification is modified as a result of the spatial distribution of the source fluxes.

The layout of the paper is as follows. In Section 2, we describe the experiments for a forced plume from a single source. A model, extending B&T, and taking account of the finite source momentum flux is given in Section 3. Experiments on two sources are discussed in Section 4 and the conclusions given in Section 5.

2. Single source experiments

2.1. Governing parameters

A source of momentum (with no buoyancy) in an enclosure leads to a turbulent jet and this provides the turbulence to keep the interior stirred and well mixed. When the source emits both buoyancy and momentum, such as a forced vent of warm or cold air, there are many possible flows depending on the directions of the momentum and buoyancy. When they act in the same direction, i.e. warm air forced upwards or cold air blown downwards, the resulting flow is a forced plume or buoyant jet. In this case, there is a competition between the buoyancy tending to stratify the interior and the momentum tending to mix it. Thus with a forced plume it is possible to go from the stratified case to the mixed case by changing the relative magnitudes of the buoyancy and momentum fluxes.

The properties of a forced plume are determined by the buoyancy flux B and the momentum flux M. If the fluid is forced through a vent of area A_S with volume flow rate Q_0 and has a density $\rho_i - \Delta\rho$ relative to the density ρ_i within the space, these fluxes at the source are defined by $B_0 = g'_0 Q_0$ and $M_0 = Q_0^2 A_S^{-1}$, where $g'_0 \equiv g\Delta\rho/\rho_0$ is the reduced gravity of the input and ρ_0 denotes the initial density within the space. For a heat source, the buoyancy flux is proportional to the heat flux, see (22). The properties of a forced plume are determined by the dimensionless parameter

$$Ar(0) = \left(\frac{L_q}{L_j}\right)^2, \tag{3}$$

where $Ar(0)$ is the source value of the Archimedes number Ar and

$$\frac{L_j}{H} = \frac{M_0^{3/4}}{HB_0^{1/2}} \tag{4}$$

and

$$\frac{L_q}{H} = \frac{Q_0}{HM_0^{1/2}}, \tag{5}$$

are dimensionless length scales associated with the effects of the initial momentum flux and volume flux, respectively, in a space of height H.

The jet-length L_j/H, sometimes known as the thermal length, gives a measure of the stratifying properties of the forced plume. A pure jet has infinite L_j/H and the interior remains unstratified for all times, while as $L_j/H \to 0$ a stratified filling box occurs. In an unconfined environment, flow above a buoyant source with a non-zero initial momentum flux is jet-like close to the source and tends towards a pure plume-like flow further above the source. A measure of the vertical height over which the flow is dominated by its source momentum flux and is essentially jet-like is called the jet-length. In a confined space, the flow may not always develop into a plume-like flow before reaching the ceiling. For $L_j \ll H$ the flow is jet-like over a relatively small vertical height and will develop into a plume-like flow well before reaching the ceiling. For $L_j \gg H$, the flow is dominated by its source momentum flux over the entire vertical height of the enclosure and will be jet-like on reaching the ceiling. The ratio L_q/H gives a measure of the height over which the initial volume flux is significant compared with that entrained by the plume. For the present experiments, L_q/H is small and the plume is well represented as a point source with zero initial volume flux. We will not discuss this parameter further.

Other dimensionless length scales of significance are the enclosure aspect ratios

$$\frac{H}{L_1} \text{ and } \frac{H}{L_2}, \tag{6}$$

Table 1
Dimensions of the plexiglass tanks

	$2L_1$ (cm)	$2L_2$ (cm)
Tank #1	61	61
Tank #2	58.3	27.9

(see Fig. 7) which determine the level of overturning induced by the enclosure geometry.

2.2. Experiments

Two plexiglass tanks were used for the experiments; one of square cross section (tank #1) and a second of rectangular cross section (tank #2, see Table 1 for dimensions). The tank was filled to a depth H with fresh water (Fig. 7). The aspect ratio of the enclosure was increased by increasing H. The nozzle, designed to produce a turbulent plume (for a schematic of the nozzle design see Hunt and Linden [5]), was suspended in the tank just below surface level; the large density step at the air/water interface provides a barrier to the flow and represents the enclosure floor.

The nozzles produced turbulent flow at the point of discharge even at relatively low supply flow rates. This enabled forced plumes with relatively small jet-lengths (see (3)) compared with H to be generated. Larger jet-lengths were achieved by reducing ϕ or increasing Q_0. For the largest jet-lengths considered, an electric pump was used to supply fluid to the nozzle.

Fluid was not removed from the tank during an experiment so that the total volume increased. The supply flow rates of the sources were negligibly small compared with the volume fluxes entrained by the sources and the relatively large cross-sectional area of the tank resulted in only a small change in the overall depth of the fluid (always less than $0.05H$) over the course of a typical experiment. This depth change had a negligible effect on the stratification and flow in the tank. To aid visualisation, dye was added to the saline solution. Fig. 7 shows schematically the enclosure and notation. The plume nozzle was located at the centre of the tank and supplied with brine via a constant-head tank to ensure a constant flow rate. The tank was diffusely lit from behind using fluorescent lighting and the experiments filmed using a video camera. Images were recorded onto video tape and simultaneously, via a frame grabber, to computer hard disk. A mirror positioned at one end of the tank at 45° to the camera enabled the flow from both the front and side of the tank to be filmed simultaneously.

The falling turbulent saline plume is dynamically equivalent to a thermal plume rising from a heat source in air and, thus, the observed flow was simply inverted, by inverting the camera, in order to represent warm air rising in a room. Using saline inputs as a model for heat sources precludes the modelling of radiative effects and, thus, we expect buoyancy gradients to be greater in the model than in a real room. Furthermore, the use of saline solutions does not allow for transfers between the fluid and the 'building' fabric and corresponds to the situation of adiabatic boundaries.

2.3. Results

We consider low aspect ratios for which overturning and mixing are negligible in the absence of source momentum flux and focus on the effect of M_0 on the initial front formation. Source conditions considered ranged from an almost pure buoyancy source ($L_j/H = 0.14$) to a highly forced buoyancy source ($L_j/H = 1.58$).

For $L_j/H = 0.14$, the formation and descent of the initial front (Fig. 2a) were as expected, similar to the pure buoyancy source case described by B&T, since the source momentum flux only affects the motion over a vertical height of the order of a jet-length. Above this height the momentum flux generated by the buoyancy exceeds M_0 and thus, on reaching the ceiling the flow is plume-like, although with a greater momentum flux than for a pure buoyancy source.

The initial stages of the flow, showing the change in scale of the overturning motion with L_j/H, are depicted schematically in Fig. 1. After colliding with the side and end walls of the enclosure the buoyant ceiling current was forced vertically downwards into the ambient layer. For small L_j/H, the downward flow was weak and only extended a small distance into the layer below. On increasing L_j/H, the length of the intrusion increased and mixing was observed as the intrusion was re-entrained by the plume, i.e. a pattern of overturning developed. The vertical scale of the overturning motion increased as L_j/H increased.

For $L_j/H \ll 1$ (Fig. 1a), the collision of the ceiling current with the walls of the enclosure produced a negligible downflow, and at the time of collision, the ceiling layer depth was comparable with the plume radius at the height of the ceiling. Wave-like motions were observed on the horizontal interface as a result of the intrusion 'slumping' back and the ceiling current reflecting off the walls. The interface was horizontal and the enclosure filled with buoyant fluid as described by B&T.

On increasing L_j/H the intrusion descended further into the layer below (Fig. 1b). Again the intrusion slumped back, but the depth of the ceiling layer formed at the end of the slumping stage, and which marked the start of the 'filling' box dynamics as described by B&T, increased as L_j/H increased. Disturbances on the interface were more pronounced as L_j/H increased. For $L_j/H \gg 1$, the intrusion extended a considerable vertical distance down the walls of the enclosure (Fig. 1c) and was re-entrained by the plume. In this case, a descending front was not observed and buoyant fluid was mixed throughout the majority of the interior.

Dye released in the plume indicated a significant radial variation in the depth of the buoyant ceiling layer during the initial development of the stratification; the layer was deepest at the perimeter of the enclosure and became pro-

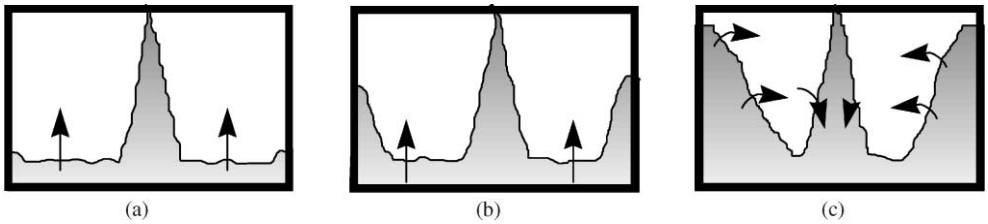

Fig. 1. Qualitative illustration of the change in scale of the initial overturning with increasing jet-length. The shaded region depicts the descending flow from the source, the lateral spreading current and intrusion at the side walls into the less dense fluid above. The jet-length increases between (a), (b) and (c). In (a) $L_j/H \ll 1$ and in (c) $L_j/H \gg 1$. Note that the scale of overturning increases with increasing L_j/H. Filling box type flows follow the situation depicted in (a) and (b). In (c), the majority of the interior subsequently becomes well mixed.

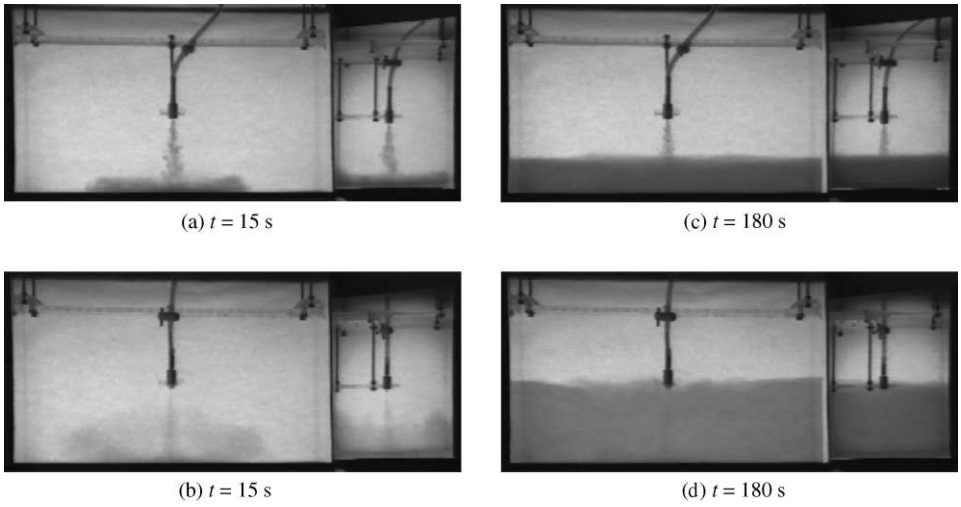

Fig. 2. Shadowgraph images of a forced saline plume with buoyancy flux $B_0 = 70.2\ \mathrm{cm^4\ s^{-3}}$ in a rectangular unventilated enclosure (tank #2, $H/L_1 = 0.5, H/L_2 = 1.05$). (a),(c) Weakly forced plume with $M_0 = 44.6\ \mathrm{cm^4\ s^{-2}}$, $L_j/H = 0.14$, and (b),(d) strongly forced plume with $M_0 = 1115.6\ \mathrm{cm^4\ s^{-2}}$, $L_j/H = 1.58$. The left portion of each image shows the flow viewed from the front of the enclosure and the right portion shows the end face of the enclosure. The 'top' of the enclosure is the free surface. Although not visible on these images it is just above the level of the source. Note that at $t = 180$ s the saline layer is deeper and less dense (as indicated by the reduced concentration of dye) in (d) than in (c).

gressively shallower towards the centre of the ceiling. For highly forced plumes, the radial increase in the depth of the initial outflow current was significantly greater than that produced by a pure plume of identical buoyancy flux. Entrainment into the radially spreading ceiling current produced by a pure buoyancy source is weak (for small aspect ratios) and the current tends to decrease in depth, or remain at approximately constant depth with increasing radius. The increase in buoyant layer depths between $L_j/H = 0.14$ and $L_j/H = 1.58$ can be seen by comparing Fig. 2c and d at 180 s. This entrainment leads to reduced upper layer temperatures with increasing L_j/H.

In the square-sectioned enclosure (tank #1, $L_1 = L_2$), the geometry is characterised by the single aspect ratio H/L_1. The two aspect ratios H/L_1 and H/L_2 describe the rectangular-sectioned enclosure (tank #2) for which $H/L_2 > H/L_1$. In the tank #2, we observed that the initial ceiling current collided with the 'front' and 'back' walls before colliding with the end walls of the enclosure (Fig. 2c and d, images at $t = 15$ s). As the current spreads laterally its depth increased rapidly as a result of shear-induced mixing and mixing caused by collision with front and back walls. A true filling box flow was observed only when both aspect ratios were less than unity and $L_j/H \ll 1$.

For sufficiently highly forced sources (Fig. 2b,d), buoyant fluid mixed throughout the entire fluid column (i.e. from ceiling to floor level) after colliding with the front and back walls before being re-entrained into the forced plume. A similar pattern was observed when the spreading current reached the left and right hand end walls. After a short time, warm air from the forced source was mixed throughout the enclosure (Fig. 2b,d).

3. Theoretical considerations for a single source

3.1. Small jet-length

For the case of $L_j/H \ll 1$, we may extend the analysis of B&T by considering a forced plume issuing from a point

source (i.e. with zero source volume flow rate) located at floor level in an insulated enclosure. By making the point source approximation we require that the volume flux added at the source is negligible compared with the volume flux entrained by the plume. The source is assumed to be away from the enclosure walls at all heights and able to entrain freely. The flow above the forced plume source may be related to the flow above a pure buoyancy source located at the virtual origin, a distance z_v behind the actual source. Morton [6] demonstrates that in the far field, the flow generated by a forced plume is equivalent to that produced by a virtual point source of buoyancy with source located a distance

$$\frac{z_v}{L_j} = \frac{1.057}{2^{5/4}\alpha^{1/2}\pi^{1/4}} \equiv G, \tag{7}$$

behind the actual source of the forced plume. With $\alpha = 0.083$ (Turner [3]), (7) reduces to $G = 1.159$. Assuming Gaussian profiles for velocity and buoyancy in the plume, the radius, momentum flux and reduced gravity as functions of the distance z from the actual source (at $z = 0$) may be expressed as

$$b = \frac{6\alpha}{5}(z + z_v), \qquad M = c_2 B_0^{2/3}(z + z_v)^{4/3} \quad \text{and}$$

$$g' = \frac{B_0^{2/3}}{c(z + z_v)^{5/3}}. \tag{8),(9),(10)}$$

where

$$c = \pi\left(\frac{5}{4\alpha}\right)^{1/3}\left(\frac{6\alpha}{5}\right)^{5/3}\left(\frac{2}{\pi}\right)^{1/3} \quad \text{and}$$

$$c_2 = \frac{\pi}{2}\left(\frac{5}{4\alpha}\right)^{2/3}\left(\frac{6\alpha}{5}\right)^{4/3}\left(\frac{2}{\pi}\right)^{2/3}, \tag{11}$$

are dimensionless constants which depend on the plume entrainment coefficient α (Morton et al. [2]). Hence, following B&T, for a *forced* plume the ratio of the inertia at the ceiling to the buoyancy of the upper layer may be written as

$$\frac{I}{\mathbf{B}} = \frac{9\alpha}{10}\left(\frac{H + z_v}{R}\right)^2 = \frac{9\alpha}{10}\left(\frac{H_{\text{eff}}}{R}\right)^2. \tag{12}$$

The 'effective' room height aspect ratio H_{eff}/R represents the room geometry in which a pure buoyancy source would produce the same flow as the forced source in a room with aspect ratio H/R. The effect of source momentum manifests itself through the virtual origin correction as a modification to the aspect ratio. For example, if momentum is added to the source of buoyancy in a space with aspect ratio H/R then the aspect ratio effectively increases to $(H + z_v)/R$. For $L_j/H < 1$, the flow will be plume-like on reaching the ceiling and, hence, increasing the effective aspect ratio by increasing the source momentum flux (and, hence, L_j) results in a larger momentum flux at the ceiling when compared with a pure plume. Substituting for (7) into (12) and taking the maximum value of $I/\mathbf{B} = 0.1$ (see B&T) we obtain an estimate of the critical jet-length required to create an overturning motion

$$\left(\frac{L_j}{H}\right)_{\text{crit}} = \frac{1}{G}\left[\frac{1}{3\alpha^{1/2}}\left(\frac{H}{R}\right)^{-1} - 1\right]. \tag{13}$$

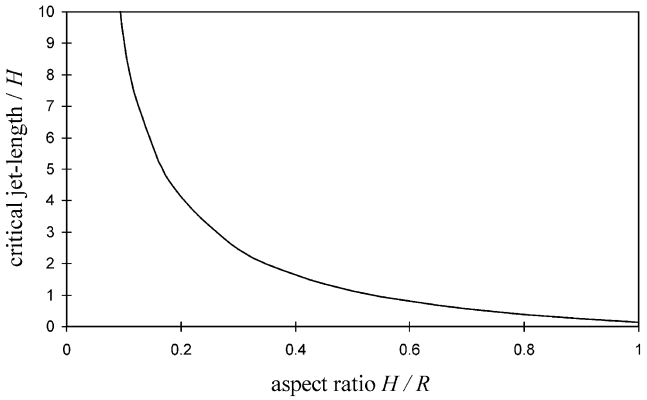

Fig. 3. The dimensionless critical jet-length plotted as a function of the room aspect ratio from (13). Above the line we expect overturning to occur and below the line we expect the interior to remain stratified at all times.

The critical jet-length (13) is plotted in Fig. 3 as a function of H/R. The figure shows that as the aspect ratio is increased the jet-length of the source must be reduced in order to maintain a stratified environment.

A simple model to predict the depth of the buoyant layer with time may be developed by introducing a time offset. We assume that, following the initial transients in which an overturning motion is generated (Fig. 1), the layer depth is not zero at time $t = 0$ as assumed by the idealised model of B&T, but rather a layer initially forms whose depth scales on the depth of the initial overturning motion. We assume further, as do B&T, that the interface subsequently descends according to the rate at which the plume supplies the layer. We now proceed by formulating an estimate of the layer depth formed by the initial overturning motion.

The momentum of the plume is assumed constant as it turns and spreads horizontally across the ceiling. The subsequent collision between the outflowing current and the side walls of the enclosure forces buoyant fluid downwards. The descending flow is buoyant and driven downwards into the denser layer by its momentum. The maximum vertical descent $d_{\max}$ of this intrusion may be estimated by modelling the intrusion as a fountain (Turner [7]),

$$d_{\max} = \sigma\frac{M_c^{3/4}}{B_c^{1/2}}, \tag{14}$$

where M_c and B_c denote the momentum and buoyancy fluxes of the current, respectively, and the dimensionless constant $\sigma = 1.85$. The volume flux at the ceiling is known from plume theory and we assume that the outflow spreads with constant depth given by the plume radius at $z = H$ (a simplification, but following a similar approach used by B&T for estimating $I/\mathbf{B}$). Then the velocity of the current U_w at the point of

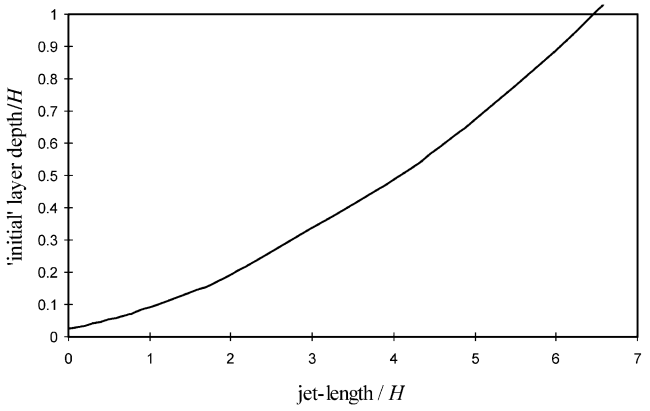

Fig. 4. The dimensionless initial layer depth $d_{\max}/H$ as a function of the dimensionless jet-length L_j/H in an enclosure of aspect ratio $H/R = 0.5$, from (16). Full overturning occurs in this case for $L_j/H \gtrsim 6.5$.

impact with the side wall is

$$U_w = \frac{5cB_0^{1/3}}{12\pi\alpha R}(H + z_v)^{2/3}. \tag{15}$$

The momentum flux $M_c = Q(H + z_v)U_w$ and from (14), we obtain

$$\frac{d_{\max}}{H} = \sigma\left(\frac{5c^2}{12\pi\alpha}\right)^{3/4}\left(1 + \frac{z_v}{H}\right)^{7/4}\left(\frac{H}{R}\right)^{3/4}. \tag{16}$$

Fig. 4 shows the variation of $d_{\max}/H$ with L_j/H in an enclosure of aspect ratio $H/R = 0.5$. From (16), we deduce that the flow down the side walls will extend as far as the floor if

$$\frac{L_j}{H} \geqslant \frac{1}{G}\left(\frac{1}{\sigma^{4/7}}\left[\frac{12\alpha\pi}{5c^2}\frac{R}{H}\right]^{3/7} - 1\right), \tag{17}$$

and for the values used in Fig. 4, this gives $L_j/H \gtrsim 6.5$.

We suppose that the buoyant layer depth takes the value $d_{\max}$ at $t = 0$, i.e. $z_0 = H - d_{\max}$ at $t = 0$. The solution of

$$\frac{dz_0}{dt} = -\frac{Q(z = z_0 + z_v)}{S}, \tag{18}$$

where S is the (constant) cross-sectional area of the enclosure, yields the interface position

$$\frac{z_0}{H} = -\frac{z_v}{H} + \left[\frac{2c}{3}\frac{t}{(H^{-2/3}B_0^{-1/3}S)} + \left(\frac{H - d_{\max} + z_v}{H}\right)^{-2/3}\right]^{-3/2}, \tag{19}$$

where $S = 4L_1L_2$ for a rectangular container and $S = \pi R^2$ for a cylindrical container. If the jet-length is zero then both $d_{\max}$ and z_v are zero and (19) reduces to the expression (1) deduced by B&T. For a given L_j/H, both z_v and $d_{\max}$ can be predicted from (7) and (16), respectively, and substituted into (19). However, from (19) we note that the ratio of the strengths of the momentum and buoyancy input at the source (as characterised by L_j) is not sufficient to determine z_0/H as the source buoyancy flux B_0 is also required.

We expect the model to overestimate the initial layer depth as not all of the plume momentum will be conserved and thus the constant of proportionality σ is likely to be lower than the value determined by Turner [7]. Interface positions deduced from (19) are plotted as a function of time in Fig. 5 for a range of source conditions.

Comparisons between measured and predicted interface heights show close agreement; Fig. 6 shows such a comparison for $L_j/H = 0.14$. Following the collision of the ceiling current with the side walls of the enclosure during the initial transients, significant wave-like motion was observed on the interface (Fig. 6 for $t \lesssim 180$ s, i.e. $t/\tau \lesssim 8.5$). During this period (19) underestimates the layer depth. At later times, (19) overestimates the layer depth, however, the differences between observed and predicted interface heights remain within 10%.

Theoretically, over the range of validity of the model (19), the interface will not reach the floor of the enclosure as zero volume flux is added at the source. Owing to the nature of the asymptotic expression (7) for the virtual origin correction, which Morton [6] gives as valid for $z/L_j \geqslant 5/(2^{5/4}\alpha^{1/2}\pi^{1/4}) \approx 5.5$ the predictions of interface height (19) are expected to be less accurate as the layer deepens. Thus, the model is only expected to be accurate for $L_j \ll H$.

3.2. Large jet-length

3.2.1. Constant buoyancy flux

For $L_j \gg H$, the interior is well-mixed and the rate of increase in the density of the interior is dependent on the rate of supply of buoyancy B_0 (independent of time) and the volume V of the enclosure:

$$\frac{dg_i'}{dt} = \frac{B_0}{V}, \tag{20}$$

where $g_i' = g(\rho_i - \rho_0)/\rho_0$ and ρ_i denotes the density of the interior at time t. For an ideal gas $g_i' \equiv g(T_i - T_0)/T_0$ where T_0 (K) and T_i denote the initial temperature of the interior and the interior temperature at time t. Integrating (20), we find that the internal temperature increases linearly with time according to

$$\frac{T_i}{T_0} = 1 + \frac{t}{t^*}, \tag{21}$$

where the characteristic time scale $t^* = gV/B_0$. The power E (W) of a heat source can be expressed in terms of a buoyancy flux via

$$B_0 = \frac{g\beta E}{\rho c_p}, \tag{22}$$

where c_p ($= 1012$ j kg^{-1} °C^{-1} at 15°C) is the specific heat of the air, β ($= 3.48 \times 10^{-3}$ °C^{-1}) is the coefficient of

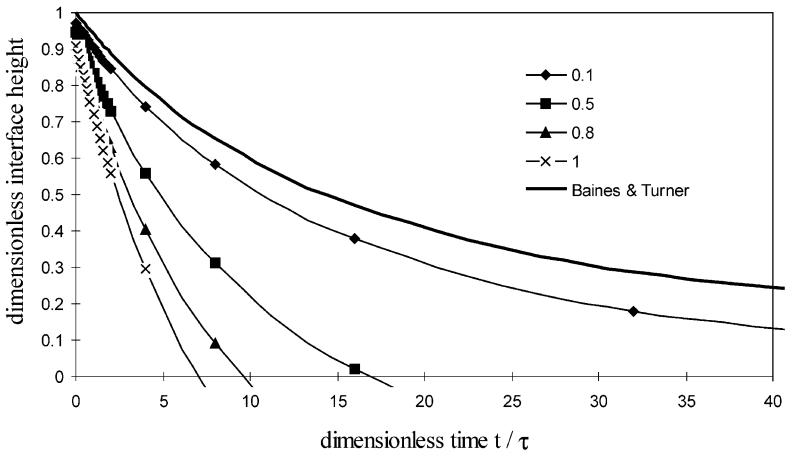

Fig. 5. The predicted interface heights z_0/H as a function of time t/τ from (19) in an enclosure of aspect ratio $H/R = 0.5$. Predictions are shown for $L_j/H = 0.1, 0.5, 0.8$ and 1, B&T's solution (1) for a pure buoyancy source is shown as the unmarked line. Note that as L_j/H increases the ascent rate of the interface increases. The time scale $\tau = H^{-2/3}B_0^{-1/3}R^2$.

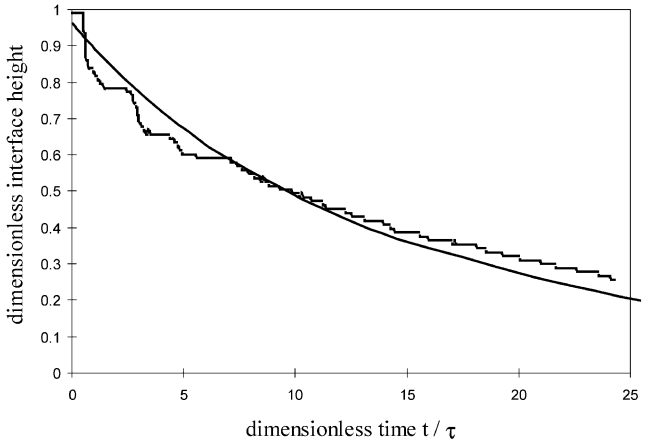

Fig. 6. Measured and predicted interface heights z_0/H as a function of time t/τ for $L_j/H = 0.14$. The data plotted is taken from the experiment shown in Fig. 2 (tank #2, $H = 14.6$ cm, $H/L_1 = 0.5$, $H/L_2 = 1.05$, $M_0 = 44.6\ \mathrm{cm^4\ s^{-2}}$, $B_0 = 70.2\ \mathrm{cm^4\ s^{-3}}$). Measurements of interface position, averaged over the half-width of the tank, were acquired at 2 s intervals during the course of the experiment—the discrete sampling accounts for the 'step-like' descent of the interface as plotted. Tank #2 has cross-sectional area $S = 1626.6\ \mathrm{cm^2}$ and hydraulic radius $R = (S/\pi)^{1/2} \approx 22.8$ cm. Predictions from (19), shown as the smooth curve, are thus with $H/R = 0.64$.

thermal expansion, and ρ ($= 1.225\ \mathrm{kg\ m^{-3}}$ at 15°C) is the density of air. In a room initially at 15°C, the time taken to increase the air temperature by 1°C is therefore

$$t_{1^\circ\mathrm{C}} = \frac{V\rho c_\mathrm{p}}{E}. \tag{23}$$

3.2.2. Non-constant buoyancy flux

In practice, if a vent supplies warm air at a constant temperature T_s then as buoyancy accumulates in the space the temperature contrast between the warm air supply and the interior $T_i(t)$ decreases. Hence, the supply buoyancy flux ($B(t) = Q_0 g'(t) = Q_0 g(T_s - T_i)/T_0$) decreases with time and a corresponding increase in L_j (from (4)) indicates that momentum effects become increasingly significant. The rate of accumulation of buoyancy may be expressed as

$$\frac{\mathrm{d}g'_\mathrm{i}}{\mathrm{d}t} = \frac{B(t)}{V}, \tag{24a}$$

or equivalently,

$$\frac{\mathrm{d}T_\mathrm{i}}{\mathrm{d}t} = \frac{Q_0}{V}(T_\mathrm{s} - T_\mathrm{i}). \tag{24b}$$

Integrating (24), and using the initial condition that $T_i = T_0$ at $t = 0$, we obtain the dependence of the interior temperature with time

$$T_\mathrm{i}(t) = T_\mathrm{s} - (T_\mathrm{s} - T_0)\mathrm{e}^{-t/t_n}, \tag{25a}$$

where $t_n = V/Q_0$ is a time constant. In terms of the reduced gravity of the interior as a fraction of the initial reduced gravity of the source (25a) may be written

$$\frac{g'_\mathrm{i}}{g'_0} = 1 - \mathrm{e}^{-t/t_n}, \tag{25b}$$

where $g'_0 = g(\rho_0 - \rho_s)/\rho_0$ is the reduced gravity of the supply at time $t = 0$; ρ_s denotes the density of the supply. For large times (25a) yields $T_i \to T_s$, i.e. the temperature of the interior tends to the temperature of the supply. From (25), the reduced gravity of the supply as a function of time is

$$\frac{g'}{g'_0} = \mathrm{e}^{-t/t_n}. \tag{26}$$

Thus, the buoyancy flux $B(t) = Q_0 g'_0 \mathrm{e}^{-t/t_n}$ and from (4) the jet-length can be written

$$L_\mathrm{j} = \frac{M_0^{3/4}}{Q_0^{1/2} g_0'^{1/2} \mathrm{e}^{-t/2t_n}}. \tag{27}$$

Hence, L_j increases with time ($L_j \to \infty$ as $t \to \infty$) and we predict that momentum effects will dominate the flow regardless of the source conditions in a finite time.

Table 2
Aspect ratios and dimensionless separation distances considered

Tank	H (cm)	Separation χ (cm)	Aspect ratio H/L_1	Aspect ratio H/L_2	χ/H
#1	15.3	28	0.5	0.5	1.83
#2	14.6	28	0.5	1.05	1.92
#2	7.3	28	0.25	0.52	3.84
#2	3.6	28	0.125	0.26	7.78
#2	14.6	16	0.5	1.05	1.10
#2	14.6	8	0.5	1.05	0.55
#2	14.6	4	0.5	1.05	0.27
#2	14.6	28	0.5	1.05	1.92

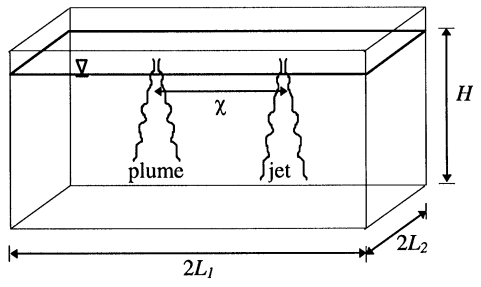

Fig. 7. Schematic diagram of the apparatus showing the two-source set-up and notation. For a single plume, the source was located at the centre of the tank cross section.

4. Two-source experiments

In this section, we examine how the stratification established by a single forced buoyancy source, with initial fluxes M_0 and B_0, is modified as a result of supplying these initial fluxes independently via two separate sources; namely, a source of momentum flux M_0 only (a jet), and a source of buoyancy flux B_0 only (a plume), and separated by a horizontal distance χ/H (Fig. 7). The dimensionless source separation χ/H is significant in determining, for example, whether the flows produced by the sources interact as they rise or whether they reach the ceiling independently. A range of separation distances (see Table 2) and relative jet/plume strengths were considered. Only the stratifications produced by simultaneously initiated inputs from the two sources are described here, although, those produced by first establishing a stable stratification and then supplying a source momentum flux, and conversely, creating a turbulent well-mixed environment by an input of momentum flux and then supplying buoyancy have also been examined.

Fresh water was supplied to the jet nozzle (of outlet diameter $\phi = 1$ or 2 mm) and coloured saline solution to the plume nozzle (nominally $\phi = 5$ mm); each supply was via a separate constant-head tank which ensured a constant volume flow rate.

For the two source experiments, the jet and plume nozzles were suspended at equal heights above the base of the tank and separated horizontally by distances of $\chi = 4, 8, 16$ or 28 cm.

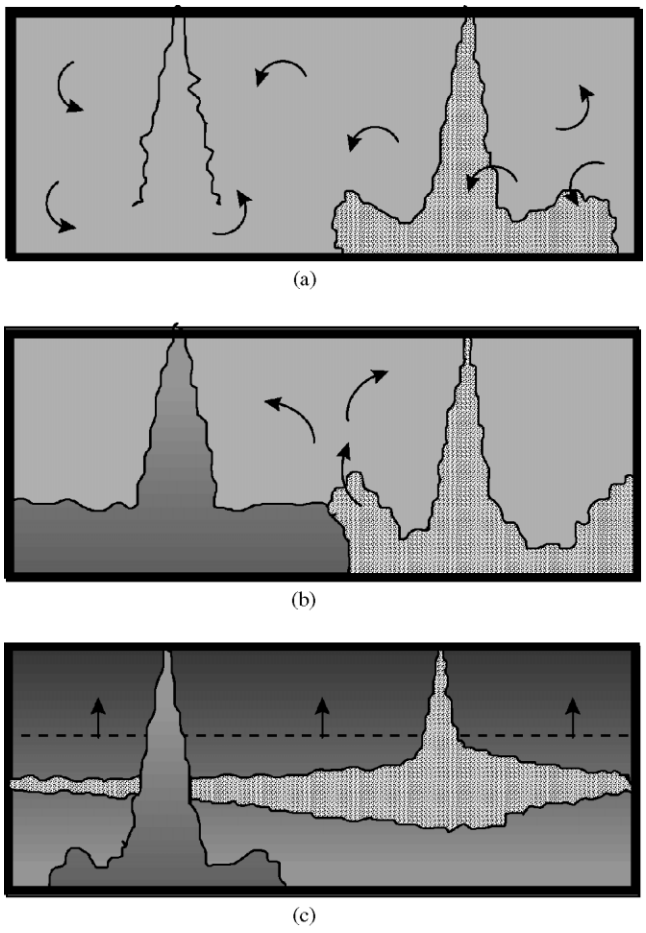

Fig. 8. Schematics of the typical flow patterns established during the experiments depending on the relative strengths of the buoyancy source (LHS) and the momentum source (RHS). (a) Weak plume; the jet flow initially dominates and creates an approximately well-mixed interior. (b) Jet and plume sources of comparable strength; buoyant fluid from the plume is removed at the collision zone and the density of the interior decreases. (c) Strong plume; the interior stably stratifies and the plume enters the stratification as a turbulent fountain. Once sufficient buoyancy has accumulated within the space the momentum source can no longer reach the base and spreads horizontally to form an intrusion. The distance between the intrusion and source decreases with time.

4.1. Effect of relative strengths of sources

Typical flow patterns within the enclosure during the initial stages of development and are illustrated schematically in Fig. 8. For a weak buoyancy source (Fig. 8a), the plume is strongly affected by the turbulence generated by the jet and a clearly defined buoyant ceiling layer is not typically formed. Buoyancy from the plume is distributed throughout the enclosure and vertical density gradients are weak.

For sources of comparable strength the typical flow pattern (Fig. 8b) has laterally spreading outflows which collide at a 'collision zone'. Here buoyant fluid is entrained by turbulent eddies created by the jet and carried downwards and mixed with the fluid below (as indicated by the arrows in Fig. 8b; note the figure depicts the flow as seen in the

laboratory and the text describes the 'inverted' picture as realised in a heated room). As a consequence, the density of the fluid originally at ambient density decreases with time.

When the jet flow is weak (Fig. 8c) the buoyancy source is able to establish and maintain a stable stratification and a 'filling box' flow develops. Once stratification has developed the jet fluid becomes dense relative to its surroundings and it has a negative buoyancy flux. The ability of the momentum source to create overturning is then further diminished. As buoyancy accumulates in the space over time, eventually the fountain will no longer have sufficient source momentum to reach the ceiling and will spread to form an intrusion (Fig. 8c) at its neutral buoyancy level. The details of the developing density stratification are then complex as the intrusion is entrained into the plume. The dynamics of a turbulent fountain are described by Turner [7] and Bloomfield and Kerr [8].

As the jet strength increases, buoyant fluid from the plume is drawn down into the lower regions of the room by the turbulence and overturning motion associated with the jet. The buoyancy is mixed throughout a larger volume of the space until, for high jet strengths, a front is not observed and buoyant fluid is mixed throughout the space. For a constant buoyancy flux, the internal temperature increases uniformly with time. The total buoyancy continues to accumulate within the space and after sufficiently large times is able to dampen out overturning motions created by the jet. In fact, regardless of the strength of the jet, the buoyancy will always dominate the motion after sufficiently large times.

Note that in the experiments the momentum source is represented as an injection of fresh water. This fluid is positively buoyant relative to the saline solution which accumulates in the tank from the saline plume and, hence, a fountain forms. In practice, the momentum source may not be associated with an input of fluid into the space, e.g., if fluid from the room were redistributed by a fan, in which case an intrusion may form if the fan directs either upwards or downwards.

4.2. Effect of source separation χ/H

For all dimensionless separation distances considered, namely, $\chi/H = 0.27$–1.9, the jet and plume flows did not interact strongly (although interaction increased as χ/H decreased), and the developing stratification was horizontally inhomogeneous. The buoyant ceiling current produced by the plume spread radially and collided with the turbulent radial ceiling jet produced by the momentum source. Where the current and ceiling jet collided there was vigorous mixing and a downward flow was observed which carried buoyant fluid into cooler air below. This fluid was re-entrained into both the rising jet and plume and a layer formed at intermediate temperature. At later times, fluid carried from the collision region had mixed throughout the entire volume and the temperature throughout the enclosure increased with time. After initially increasing in depth, the buoyant layer approached a steady depth, indicating that the rate of removal of fluid from this layer (at the collision region) was matched by the rate of fluid supplied to the layer by the plume and jet. The steady layer depth, which increased with increasing H, was comparable with the plume width at the ceiling. Fig. 9 shows the saline stratification at 90 s for $\chi/H = 1.9$ and $\chi/H = 0.27$.

Note that the flow was more symmetric (about the vertical axis midway between the sources) at the smaller separation and, in addition, the horizontal variation in density is reduced (as indicated by the concentration of the dye). This trend might be expected to continue and, for sufficiently small χ/H, the motion is anticipated to be similar to that established by a single forced plume with the combined fluxes M_0 and B_0. Further experiments are planned to examine in detail the transition from two-source to single-source behaviour. Similar flows were observed in both square and rectangular section enclosures.

4.3. Effect of aspect ratio

Aspect ratios of $H/L_1 = 0.5$ (Fig. 10a), 0.25 (Fig. 10b) and 0.125, with a source separation of $\chi/H = 1.9$ were considered. At each aspect ratio, the ascending flows from the sources remained separate and did not strongly interact and mix. On reaching the ceiling, the horizontal outflows from sources collided (as described above) and buoyant fluid from the plume outflow was carried downwards and mixed throughout the enclosure. The degree of overturning decreased as the aspect ratio decreased. With an aspect ratio of $H/L_1 = 0.5$ the outflows collided roughly at the midpoint between the jet and plume centre-lines (Fig. 10a). As the aspect ratio decreased the collision occurred closer to the jet centre-line. The stable buoyant layer fed by the plume initially increased in depth and intruded further across the ceiling toward the origin of the turbulent ceiling jet flow. For the smaller aspect ratios considered buoyant fluid was observed to spread above the opposing ceiling jet and the buoyant layer extended across the entire surface area of the ceiling (Fig. 10b).

5. Conclusions

We have described results of an experimental study that examines the stratification established by a localised buoyant source of non-zero source momentum flux on the floor in a closed room of aspect ratio (H/L) less than unity. In the absence of source momentum flux, a stably stratified region of warm air forms at the ceiling separated by a horizontal interface from the cooler air below. The descent of the interface is initially rapid and the rate of descent decreases as the enclosure fills. Increasing the source momentum flux leads to increased mixing and overturning motion, and as a result the warm air layer descends more rapidly than for the

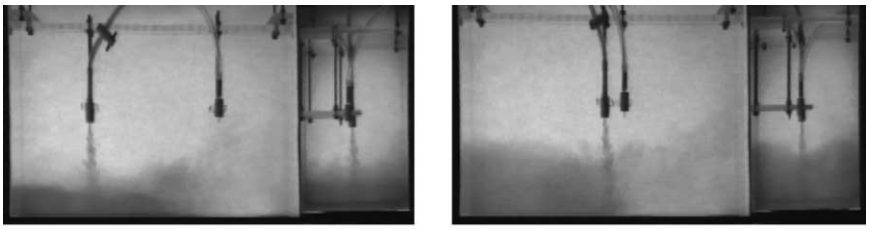

(a) $\chi/H = 1.9$ (b) $\chi/H = 0.27$

Fig. 9. Localised buoyancy source (saline plume, LHS) and momentum source (water jet, RHS) in an unventilated enclosure. The flow is shown at 90 s. For the jet $M_0 = 1115.6\ \mathrm{cm^4\ s^{-2}}$; for the (weakly forced) plume $M_0 = 44.6\ \mathrm{cm^4\ s^{-2}}$ and $B_0 = 70.2\ \mathrm{cm^4\ s^{-3}}$. Tank #2 with $H/L_1 = 0.5$, $H/L_2 = 1.05$.

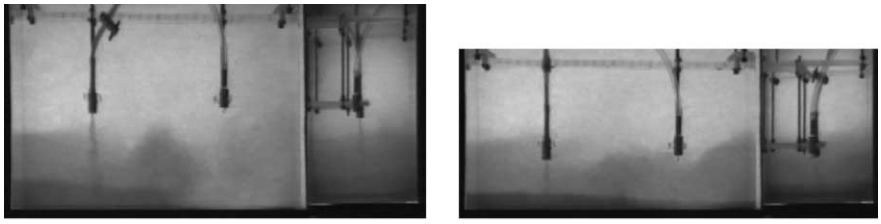

(a) $H/L_1 = 0.5$ (b) $H/L_1 = 0.25$

Fig. 10. Localised buoyancy source (saline plume, LHS) and momentum source (water jet, RHS) in an unventilated enclosure. The flow is shown at 180 s. For the jet $M_0 = 1115.6\ \mathrm{cm^4\ s^{-2}}$; for the (weakly forced) plume $M_0 = 44.6\ \mathrm{cm^4\ s^{-2}}$ and $B_0 = 70.2\ \mathrm{cm^4\ s^{-3}}$. Tank #2 with $\chi/H = 1.9$. In (a) $H/L_2 = 1.05$ and in (b) $H/L_2 = 0.52$.

zero momentum flux case and is on average cooler. Baines and Turner [1] observed that the scale of overturning motion increased with increasing aspect ratio and thus, the qualitative effect of increasing M_0 is equivalent to increasing the aspect ratio of the space. The vertical scale of the overturning motion is characterised by the dimensionless jet-length and aspect ratio of the enclosure. If two characteristic horizontal length scales are available, e.g., in a room of rectangular cross-section, the smaller of the aspect ratios determines the initial extent of the overturning motion. For source jet-lengths $L_j/H \ll 1$, the motion inside the enclosure was well described by the filling box model of B&T with the finite momentum flux treated by considering that the plume rises from a virtual origin. The interior is stably stratified and the temperature and the vertical temperature gradient increase linearly with time.

For source conditions which yield jet-lengths sufficiently larger than the room height, the heat from the source is distributed throughout the enclosure by the momentum of the plume and a horizontal descending initial front was not observed. There are two distinct possibilities depending on the nature of the heat input. If a constant heat flux is maintained, the effects of the momentum flux diminish with time and the interior stratifies. The form of the stratification is then determined by the small L_j/H limit at large times and the temperature of the interior increases continuously. On the other hand, if the input is such that a constant supply temperature is maintained, the interior remains well-mixed at all times and eventually reaches the supply temperature.

When buoyancy and momentum fluxes are input from separate sources, the developing thermal stratification is different from that established by an equivalent single source. The initial mixing produced by the momentum source depends critically on the separation and relative strengths of the sources. At large times, a constant heat input produces a stratification irrespective of the momentum flux of the jet.

This study has explored the effects of the combined effects of sources of buoyancy and momentum in a single space. We have focused here on the forms of the stratification that form under idealised conditions, with the aim of isolating the competing effects of the stratifying influences of the buoyancy input and the mixing effects of the momentum input. In a real building other effects will influence the stratification, notably radiation and heat transfers between the walls and the interior air. However, these are unlikely to alter the basic flow patterns described here, since they tend to be smoothing effects which are partly a response to the stratification set up by the internal sources. One significant exception would be the case of a cool ceiling which would produce convection on contact with the warm ceiling layer. Generally, we would expect this to reduce the stratification and lead to a more mixed state than for an adiabatic ceiling.

Acknowledgements

The experiments were performed at the Department of Mechanical & Aerospace Engineering at the University of

California, San Diego, USA. G.R.H. and P.C. gratefully acknowledge the funding of the EPSRC. G.R.H. was supported as a Research Associate and P.C. as a Visiting Fellow.

References

[1] Baines WD, Turner JS. Turbulent buoyant convection from a source in a confined region. Journal of Fluid Mechanics 1968;37:51–80.
[2] Morton BR, Taylor GI, Turner JS. Turbulent gravitational convection from maintained and instantaneous sources. Proceedings of the Royal Society A 1956;234:1–23.
[3] Turner JS. Turbulent entrainment: the development of the entrainment assumption, and its application to geophysical flows. Journal of Fluid Mechanics 1986;173:431–71.
[4] Barnett SJ. The dynamics of buoyant releases in confined spaces. Ph.D. thesis. The University of Cambridge, 1991, 166 pp.
[5] Hunt GR, Linden PF. Steady-state flows in an enclosure ventilated by buoyancy forces assisted by wind. Journal of Fluid Mechanics 2001;426:355–86.
[6] Morton BR. Forced plumes. Journal of Fluid Mechanics 1959;5: 151–63.
[7] Turner JS. Jets and plumes with negative or reversing buoyancy. Journal of Fluid Mechanics 1966;26:779–92.
[8] Bloomfield LJ, Kerr RC. Turbulent fountains in a stratified fluid. Journal of Fluid Mechanics 1998;385:335–56.